Journal of Integrative Agriculture 2026, 25(7): 2701–2713

Available online at ScienceDirect

Journal of Integrative Agriculture



RESEARCH ARTICLE

Filament-like plant protein 7 (*FPP7*) negatively regulates rice salt tolerance by enhancing abscisic acid sensitivity and disturbing sodium and ROS homeostasis

Fan Fan[1*], Jin Chen[3*], Lingyue Yan[1], Wenjie Hu[1], Xue Liu[1], Jia Zeng[4], Ling Liu[1], Ting Liu[1], Nenghui Ye[1#], Dingyang Yuan[3#], Meijuan Duan[1, 2#]

[1] *College of Agriculture, Hunan Agricultural University, Changsha 410128, China*
[2] *Yuelushan Laboratory, Changsha 410128, China*
[3] *State Key Laboratory of Hybrid Rice/Hunan Hybrid Rice Research Center, Hunan Academy of Agricultural Sciences, Changsha 410125, China*
[4] *Longping Branch, College of Biology, Hunan University, Changsha 410125, China*

Highlights

- First identification of 59 filament-like plant proteins (FPP) genes across six plant species, revealing their conserved evolutionary patterns in monocots.
- The rice *OsFPP7* gene negatively regulates salt tolerance, impacting seed germination and seedling growth.
- OsFPP7 influences rice salt tolerance by regulating abscisic acid signaling, ion homeostasis, and reactive oxygen species balance.

Abstract

Filament-like plant proteins are intermediate filament proteins that play a major role in the development and growth of plants. However, no studies have systematically identified or characterized the filament-like plant proteins (FPP) family in plants. Fifty-nine FPP candidates were found in this study by analyzing the genomes of two dicots and four monocots. Phylogenetic analysis and multicollinearity mapping showed the relatively conserved evolution of FPP genes in monocots. In rice, eight *OsFPPs* were characterized and found to be induced or repressed by abiotic stresses. Additional genetic evidence showed that *OsFPP7*-overexpressing rice exhibited increased sensitivity to abscisic acid during the germination stage, disrupted Na^+/K^+ homeostasis, and disrupted balance of reactive oxygen species during the seedling stage when exposed to salt stress. Conversely, the knockout of *OsFPP7* alleviated abscisic acid (ABA) sensitivity, safeguarded the antioxidant system and sodium ion transport system, and thus enhanced rice salt tolerance. In the cytoskeleton, the functions of FPPs in controlling salt stress and plant stress tolerance mechanisms are all further elucidated by our findings.

Keywords: OsFPP7, abscisic acid, Na^+ homeostasis, reactive oxygen species homeostasis, rice (*Oryza sativa* L.)

1. Introduction

The productivity and growth of crops are restricted by salinity, which is one of the most challenging environmental factors to manage (Negrão *et al.* 2011). Salinized soil is widely distributed in more than 100 countries worldwide, with a total area of approximately 955 million ha (Flowers and Yeo 1995), and China accounts for 99.13 million ha (Zhang 2007). Rice (*Oryza sativa* L.) is one of the most important grain crops, as it provides a fundamental source of food for over 50% of the world's population (Sasaki and Burr 2000). China is the biggest consumer and producer of rice on earth, with over 300,000 km^2 planted annually (Xu *et al.* 2021). Most physiological and metabolic processes in rice are affected to varying degrees by salt stress. Such disruptions include the inhibition of plant seed germination, delay in plant growth,

Received 2 May 2024; Received in revised form 24 June 2024; Accepted 1 July 2024; Available online 30 August 2024
Fan Fan, E-mail: fanfanchn9@163.com; Jin Chen, E-mail: jinchen_0704@163.com; #Correspondence Nenghui Ye, E-mail: nye@hunau.edu.cn; Dingyang Yuan, E-mail: yuandingyang@hhrrc.ac.cn; Meijuan Duan, E-mail: duanmeijuan@163.com
* These authors contributed equally to this study.

© 2026 CAAS. Publishing services by Elsevier B.V. on behalf of KeAi Communications Co. Ltd. This is an open access article under the CC BY-NC-ND license (http://creativecommons.org/licenses/by-nc-nd/4.0/). Peer review under responsibility of Editorial Board of *Journal of Integrative Agriculture*.
doi: 10.1016/j.jia.2024.08.029

weakening of plant photosynthesis, and premature aging of plants, which ultimately influence yield (Hussain *et al.* 2018). As a result, it is crucial to uncover the mechanisms of salt-tolerant crops and develop new rice varieties that can sustainably produce food in salinized environments.

Coiled-coils (CCs) are formed by two or more α-helices winding and looping around each other, and they serve as oligomerization domains for transcription factors (TFs), motor proteins, and structural proteins. Two types of CC proteins can be distinguished by their "long" or "short" CC domains (Rose *et al.* 2004). Long coiled-coil (LCC) proteins act as platforms and scaffolds with hundreds of amino acids, and they connect the cellular processes in various species (Gindullis *et al.* 2002; Bassham *et al.* 2013). A significant portion of LCC proteins are specific to plants, such as *weak chloroplast movement under blue light1*, MAR-binding filament-like protein1 (*MFP1*), *CONSTITUTIVE PHOTOMORPHOGENIC1* (*COP1*), and *COP1-interacting protein1*, and *COP1-interacting protein1* is involved in several eukaryotic cell organizing and regulatory functions (Rose *et al.* 2005). Furthermore, two *Arabidopsis* LCC proteins, PICC (PAMP-INDUCED) and PICL (PICC-LIKE), exhibit increased sensitivity in their double mutants during post-germination development in response to abscisic acid (ABA) (Bassham *et al.* 2013).

Among the LCC proteins of the cytoskeleton, the intermediate filament (IF) proteins are engaged in cytoskeletal motor protein function, nuclear organization, and organelle architecture. Furthermore, recent studies have shown that IFs are not only fundamental to cellular structure but also key elements in cell signaling, stress sensing, and integrating defense responses (Pérez-Sala and Quinlan 2024). Nuclear lamins, known as type V IF proteins, play essential roles in nuclear envelope (NE) assembly, DNA synthesis, gene regulation, apoptosis, and providing structural support for the nucleus. They polymerize into intricate filamentous mesh networks near the nuclear periphery (De Vos *et al.* 2011). Lamin expression and stability are regulated by oxidative stress. Reactive oxygen species (ROS) production is the primary cause of oxidative stress, which also leads to cell death, senescence, and heightened susceptibility to ROS (Shimi and Goldman 2014). The three lamin genes in mammals (*LMNB2*, *LMNB1*, and *LMNA*) form seven variably spliced isoforms that are relevant to various laminopathies (De Vos *et al.* 2011). The expression levels of antioxidant enzymes, such as superoxide dismutase (SOD), glutathione peroxidase (GPX), catalase (CAT), and glutathione (GSH)-S-transferase (GST), are influenced by laminopathies (Mao *et al.* 2020). For example, Hutchinson-Gilford progeria syndrome is a type of laminopathy characterized by a protein deficiency in fibroblasts that targets peroxisomes. Due to the abundance of catalytic enzymes, peroxisomes are membrane-covered subcellular structures that are essential for scavenging ROS (Mao *et al.* 2020). Altering lamin expression to modulate ROS metabolism may provide a biological basis for developing therapeutic strategies that target impeding the initiation, progression, and metastasis of cancer (Shimi and Goldman 2014).

Previous research has suggested a lack of homology in plant lamins. However, MAR-binding proteins (MARBPs), *MFP1*, *NMCP1*, nuclear matrix protein 1 (NMP1), and keratin-like proteins exhibit structures similar to that of lamin (Clark *et al.* 2004). In rice, OsNMCP1 interacts with the chromatin remodeler OsSWI3C to modulate chromatin accessibility, which in turn controls drought tolerance and root growth (Yang *et al.* 2020). Like large filament nuclear proteins in mammals, MFP1 is a large membrane-related protein that binds to MARs *via* a CC structure. It attaches to chromatin and is involved in organizing decondensed chromatin and signaling (Samaniego *et al.* 2008). It is also a nuclear DNA-binding protein that has been identified in *Arabidopsis*, tobacco, *Allium cepa*, and tomato cells (Patel *et al.* 2005; Samaniego *et al.* 2008). In *Arabidopsis* chloroplasts, *MFP1* is also necessary for the appropriate initiation of starch granule formation (Seung *et al.* 2018).

Furthermore, other possible components have been suggested for the higher plant lamina. The earliest class of plant-specific LCC proteins, called filament-like plant proteins (FPPs), was identified in the *Arabidopsis* genome. A non-CC linker separates the two clusters of LCC domains and four unique sequence motifs (Gindullis *et al.* 2002; Rose *et al.* 2004). All FPPs encode the DUF869 domain with an unknown function, while AtFPP4 encodes a microtubule-binding protein that controls microtubule stability and trichome cell shape by interacting with ZWICHEL/KCBP (Chen *et al.* 2016). Although *AtFPP1/VETH3* is not up-regulated in root xylem cells, proper secondary cell wall deposition is ensured by *AtFPP2* and *AtFPP3*, which are expressed specifically in developing root xylem cells and recruit *EXO70A1* to cortical microtubules (Oda *et al.* 2015). LeFPP interacts with LeMAF1, which is a NE-associated protein. In addition, MAF1 was found to operate as a master regulator of Pol III-dependent transcription, which coordinates the inhibition of lipid metabolism, tumor development, and RNA synthesis in animals (Gindullis *et al.* 2002; Johnson and Stiles 2016).

In general, FPPs are crucial for proper development and growth. However, their role in regulating stress resistance in rice is not known. This study examined the expression patterns, evolution, collinearity, and categorization of eight *OsFPPs* in rice. On this basis, we confirmed that *OsFPP7* functions as a negative modulator of rice salt resistance by controlling ABA sensitivity during the budding stage, as well as Na^+/K^+ homeostasis and ROS homeostasis throughout the seedling stages.

2. Materials and methods

2.1. Filament-like plant protein family gene identification and characterization

Sequences with the filament-like plant protein family (PF05911) domain in their the Hidden Markov Model (HMM) profiles were acquired from the Pfam database (https://pfam.xfam.org/). Then from the Ensembl Plants website (http://plants.ensembl.org/index.html), the general feature format (GFF) files and genomic data were obtained for the following species: rice (*Oryza sativa* L.), maize (*Zea mays* L.), soybean (*Glycine max* L.), barley (*Hordeum vulgare* L.), *Arabidopsis* (*Arabidopsis thaliana* L.), and wheat (*Triticum aestivum*

L.). Based on criteria of bits>100, and E-value≤1e^{-5}, these profiles were used as the reference canonical domains for HMM searching for analogs by employing the HMMER 3.3.1 website (http://hmmer.org/download.html) (Sonnhammer *et al.* 1997).

2.2. Alignment and phylogenetic tree of FPPs

The pairwise deletion, Jones-Taylor-Thornton Model, 1,000 bootstrap method, and other parameters were used to analyze the multiple sequence alignment of the FPPs using the default parameter settings of MEGA11. Then, using the Neighbor-Joining method, the various compared files that were generated were uploaded into MEGA11 to determine phylogenetic relationships. Ultimately, the phylogenetic tree was categorized, elucidated, and managed using the Evolview web application (http://www.evolgenius.info/evolview/#/treeview).

2.3. Collinearity relationship analysis

The genome sequence data and genome organization annotation data were analyzed using TBtools software's One Step MCScanX (Chen *et al.* 2020) to determine the collinearity of FPPs across every pair of species. The resulting files were then imported into File Merge for MCScanX to establish any predetermined collinearity connections among all members of the FPP family. Finally, the homology data was graphed and visualized using the Multiple Synteny Plot in TBtools.

2.4. Bioinformatic analysis of OsFPPs

The ExPASy online ProtParam tool (http://www.expasy.org/protparam/) was used to determine the fundamental physical and chemical characteristics of OsFPPs, such as the open reading frame, isoelectric point (pI), aliphatic index, instability index, molecular weight (MW), GRAVY, and number of amino acids for each filament-like plant proteins (FPP) gene. Furthermore, the WoLP PSORT online platform (https://wolfpsort.hgc.jp/) was used to forecast the subcellular distributions of the OsFPPs.

Utilizing TBtools (Chen e*t al.* 2020), exon position and gene length comparisons were made to create the exon/intron structures. This process was carried out using the entire genome and the associated coding sequences that were retrieved, as previously demonstrated. Conserved domains were predicted on the NCBI-CDD website (http://www.ncbi.nlm.nih.gov/Structure/cdd/wrpsb.cgi). Exon–intron architectures were predicted using the coding sequences of *OsFPPs* and the matching genomic sequences. Protein domains were assessed *via* SMART (http://smart.embl-heidelberg.de/). The online MEME v5.1.1 tool was adapted to study the conserved motifs of *OsFPPs*. Using TBtools software, conserved motifs and a schematic diagram of the gene architectures were displayed and revised. PlantCARE was used to analyze the 2,000 bp sequences upstream of the *OsFPPs* translation start codons, and the results were displayed *via* the TBtools software. To predict protein interactions associated with members of the FPP family, a species source selection model using *Arabidopsis* and rice was employed through the functional protein association web online database STRING (https://string-db.org).

2.5. *OsFPP* expression pattern analysis under abiotic and biotic stress conditions

Cold, drought, flood, ABA, methyl jasmonate response element (MeJA), and salicylic acid (SA) transcriptome data used for the gene expression analysis were acquired from RiceXPro (https://ricexpro.dna.affrc.go.jp). The heat maps were created using TBtools software, and the gene expression levels were denoted by fragments per kilobase of exon per million fragments mapped (FPKM) (Chen *et al.* 2020).

2.6. Plant materials and growth environments

A vector for *OsFPP7* overexpression (OE) was created by amplifying the whole CDS of *OsFPP7* from Nipponbare cDNA and cloning it into the binary vector pC1390U. CRISPR-Cas9-mediated gene editing was used to create *OsFPP7* knock-out mutants by a previously reported protocol (Lu *et al.* 2020). Using CRISPRP 2.0 (http://crispr.hzau.edu.cn/CRISPR2/), single-guide RNAs were designed and added to the pCBSG032 vector. In this study, every mutant and OE line employed was based on the ZH11 (*japonica* variety, WT) background.

Thirty germinated rice seeds were arranged on a sprouting box for stress treatment during the germination stage, and 10 μmol L^{-1} ABA, 100 mmo L^{-1} NaCl, or both were applied to the seeds, with water treatment serving as the control. After 10 d of growth at 28°C under a 14-h light/10-h dark cycle, the fresh weights, shoot lengths, and root lengths of the seedlings were measured. For stress treatment in the seedling stage, 2-wk-old seedlings were placed into Yoshida's culture solution, which contained 0 or 150 mmol L^{-1} NaCl, at 28°C under 16 h of light and 8 h of darkness in a temperature-controlled growth environment for 20 d. Then the seedlings were returned to a salt-free solution for a 7-d recovery period. At least three repetitions of the experiments produced comparable outcomes. For agronomic trait investigations, all materials were planted in the experimental field under natural long-day conditions at the transgenic test base in Changsha, China.

2.7. RNA extraction and quantification

Total RNA was extracted from rice tissues using the TransZol Up Plus RNA Kit (TransGen Biotech, Beijing, China). A NanoDrop 2000 spectrophotometer (Thermo Fisher Scientific, USA) was used to assess the purity and quantification of RNA. For RT-PCR, 1 μg of total RNA that had been processed with DNase I was used to synthesize cDNA using the RevertAid First Strand cDNA Synthesis Kit (Thermo Fisher Scientific, USA). A total of 1 μg of total RNA was reverse transcribed into cDNA through the All-in-One First-Strand cDNA Synthesis SuperMix for qRT-PCR with gDNA remover (TransGen Biotech, Beijing, China). Using the TB Green® Premix Ex Taq™ II (Tli RNaseH Plus) (TaKaRa, Japan) methodology and the Roche Light Cycler 480 System (Roche, Switzerland), the cDNA library generated was used as a template for qRT-PCR analysis. For each treatment, the relative gene expression levels were calculated using the $2^{-\Delta\Delta C_T}$ technique

with three biological replicates. The rice ubiquitin gene (LOC_*Os03g13170*) was applied as the internal control. The primer sequences for qRT-PCR are provided in Appendix A.

2.8. Subcellular localization analysis

A PHB-OsFPP7-YFP recombinant plasmid was produced by amplifying the OsFPP7 CDS and inserting it into the PHB-X-YFP vector. The cell membrane marker *HKT1;1* and the nuclear marker *BZIP52* were inserted into the PHB-X-CFP vector, respectively. A variety of combinations were inserted into the GV3101 strain (Weidi, Shanghai, China) and then infiltrated into the tobacco (*Nicotiana benthamiana*) plants that were 4–6 wk old on the abaxial side. An LSM880 Confocal Microscope (Zeiss, Oberkochen, Germany) was used to detect the fluorescence signals. The primers used in the subcellular localization assay can be found in Appendix A.

2.9. Yeast self-activation assay pGBKT7(BD)

After amplifying the OsFPP7 CDS and inserting it into the $pGBKT_7$ vector, the empty $pGBKT_7$ plasmid and the constructed plasmid were transformed into the AH109 yeast strain. Transformation with the empty $pGBKT_7$ was used as a negative control. The OD_{600} was adjusted to 0.0002, and drops were placed on SD/–His–Trp–Ade and SD/–Trp media. The yeast clones were then grown upside down at 30°C for 3–5 d. Appendix A lists the primers used in the yeast self-activation assay.

2.10. DAB and NBT staining

Staining assays with DAB (3,3'-diaminobenzidine tetrahydrochloride) and NBT (nitrotetrazolium blue chloride) were performed either with or without 150 mmol L^{-1} NaCl for 24 h on 2-wk-old seedlings. NBT staining was carried out as previously described (Stefano and Piera 2001). Diaminobenzidine (DAB) staining was carried out through a DAB Enhanced Substrate Kit (Solarbio, Beijing, China), with reference to the manufacturer's instructions. A representative set of data is presented below based on three biological replicates, with each replicate consisting of 20 independent plants.

2.11. Physiological and biochemical analyses

Seedlings that were 2 wk old were treated with 0 or 150 mmol L^{-1} NaCl for either 24 h or 5 d. After the plants were exposed to salinity for 24 h, the activities of CAT, SOD, and POD were measured by referring to the manufacturer's protocol of the Corresponding Assay Kit (Solarbio, Beijing, China). After 5 d, the contents of soluble sugar and MDA were measured according to the manufacturer's protocol of the Corresponding Assay Kit (Solarbio, Beijing, China).

2.12. Statistical analysis

The two-tailed Student's *t*-test was employed to determine significant differences using IBM SPSS in the statistical analysis between the WT and transgenic lines. The *P*-values were considered statistically significant when they were less than 0.05. GraphPad Prism 8 was used to generate figures (GraphPad, USA). The relevant figure legends include information about the biological replicates, including numbers and specific details.

3. Results

3.1. Identification of FPP family genes throughout the genome

From the genomes of four monocots (*Oryza sativa* L., *Triticum aestivum* L., *Hordeum vulgare* L., and *Zea mays* L.), totals of 8, 18, 6, and 10 FPPs were found, respectively (Appendix B). In addition, nine and eight FPPs were detected from two dicots (*Glycine max* L. and *Arabidopsis thaliana* L., respectively). The FPP family can be divided into three main groupings according to evolutionary studies. Group I includes Ia and Ib, while Group III contains IIIa, IIIb, and IIIc. Most *AtFPPs* and *GlyFPPs* are strongly clustered together (Fig. 1-A), indicating that each family and genus share similar evolutionary histories. The OsFPP proteins were highly clustered with *TvFPPs*, *ZmFPPs*, and *HvFPPs*, all of which were evenly distributed in each group. Collinearity analysis showed that 24, 15, and 9 pairs were found between rice and wheat, maize, and barley, respectively (Fig. 1-B), while no collinear gene pairs were detected between rice and either *Arabidopsis* or soybean (Appendix C). These results suggest that *OsFPPs* exhibit significant genomic synteny with the three other monocots, but no collinearity was observed between rice and the two dicots in this study.

The FPP family members identified from rice were further characterized as provided in Appendix D. Every *OsFPP* was found in the nucleus, except for LOC_*Os04g42610*, which was found in the chloroplast. The FPPs have protein molecular weights (MWs) between 84.62 and 115.92 kD, with sequence lengths ranging from 725 to 1,041 aa. The OsFPP proteins have isoelectric values ranging between 4.92 and 6.09, which is similar to the range of most proteins. All *OsFPPs* have GRAVY values less than zero, indicating that they are hydrophilic. The *OsFPPs* were identified as unstable proteins, with instability index values all greater than 40. The aliphatic index was used to evaluate the solubility and antioxidant properties of the proteins, and the values of all *FPPs* ranged from 74.05 to 88.59. Our analysis revealed that the *OsFPPs* are unstable and hydrophilic. To determine the links between the *OsFPP* genes and potential gene duplication events, syntenic blocks within the rice genome were investigated. The expansion of the *OsFPP* family was likely facilitated by segmental duplications in these regions, as evidenced by the involvement of four *OsFPPs* in two separate duplication events on different chromosomes (Appendix E).

3.2. *cis*-Regulatory element analysis, conserved motifs, and gene structures of the *OsFPPs* genes

The *cis*-regulatory elements, conserved motifs, conserved domains, phylogenetic relationships, and gene structures were examined to understand the formation and development of the *OsFPP* family (Fig. 2; Appendix F). In general, most motifs clustered in the same evolutionary taxon possess a common composition pattern, as indicated by conservative motif analysis. In this study, all *OsFPPs* have the same six

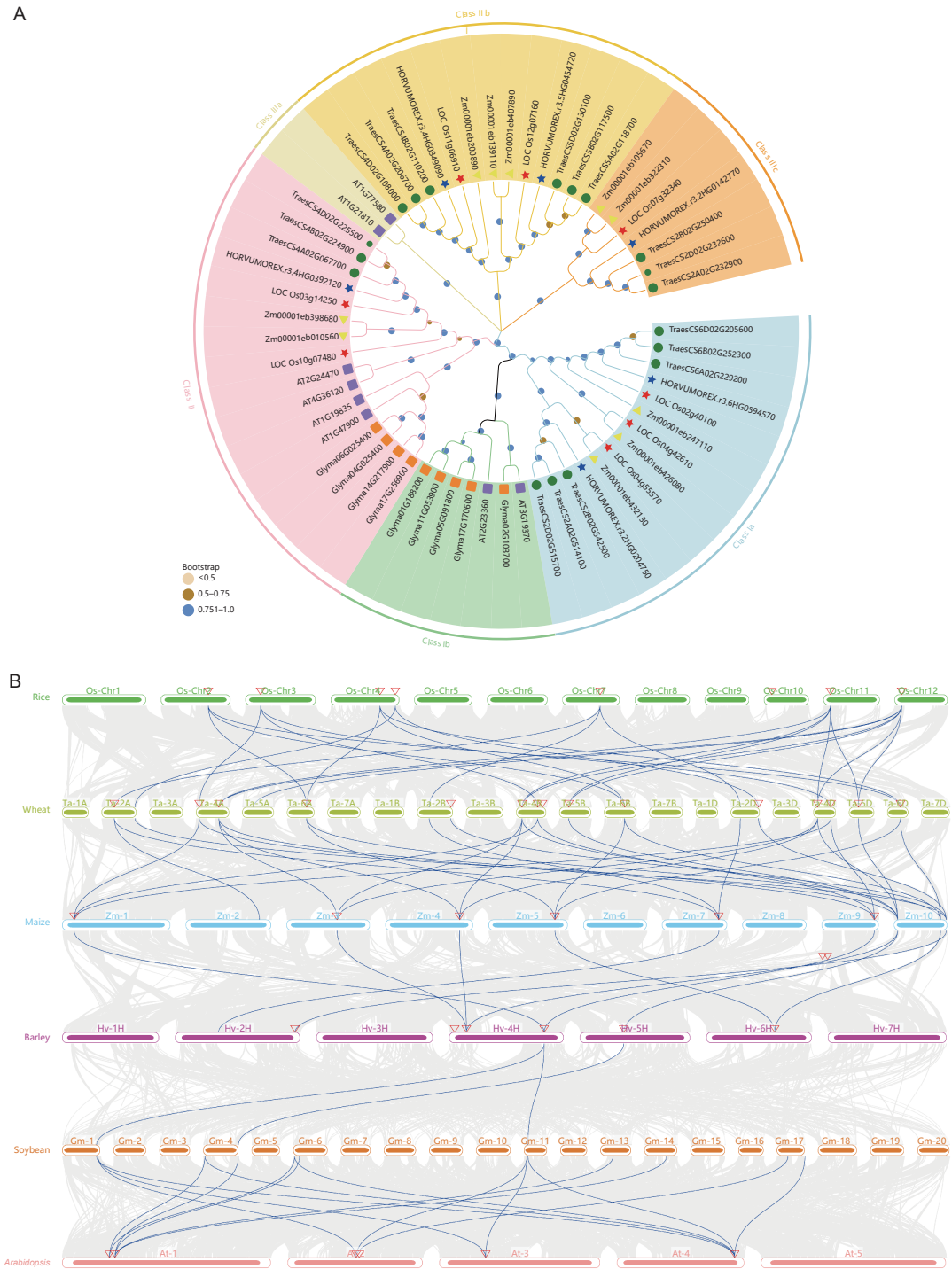


Fig. 1 Phylogenetic and collinearity analyses of filament-like plant proteins (FPPs) in rice, wheat, maize, barley, soybean, and *Arabidopsis*. A, phylogenetic relationships of FPPs. Clusters I–III are displayed in different colors. Each cluster is divided into different subgroups (a–c) based on their evolutionary distances. Symbols with different colors and shapes represent various species. B, collinearity analysis of FPPs. Different species are represented by various colors. Gray lines in the background represent the orthologous genes of neighboring species, while blue lines indicate the duplicate FPP gene pairs with collinearity links. The number assigned to each chromosome is shown above it.

motifs, and two additional motifs are present in more than half of them. Protein structure and distribution analysis revealed that *OsFPPs* possess 1–4 FPP domains. The molecular or cellular function of a protein may be partially or fully revealed by its conserved domain footprint, and that function may be precisely identified by the protein's domain architecture. Most *OsFPPs* contain the FPP superfamily domain, and only two have the FPP domain (Fig. 2-C). The *OsFPPs* possess 3–5 exons, and one or two introns are present in the 5′-untranslated region (UTR), except for LOC_*Os10g07480*

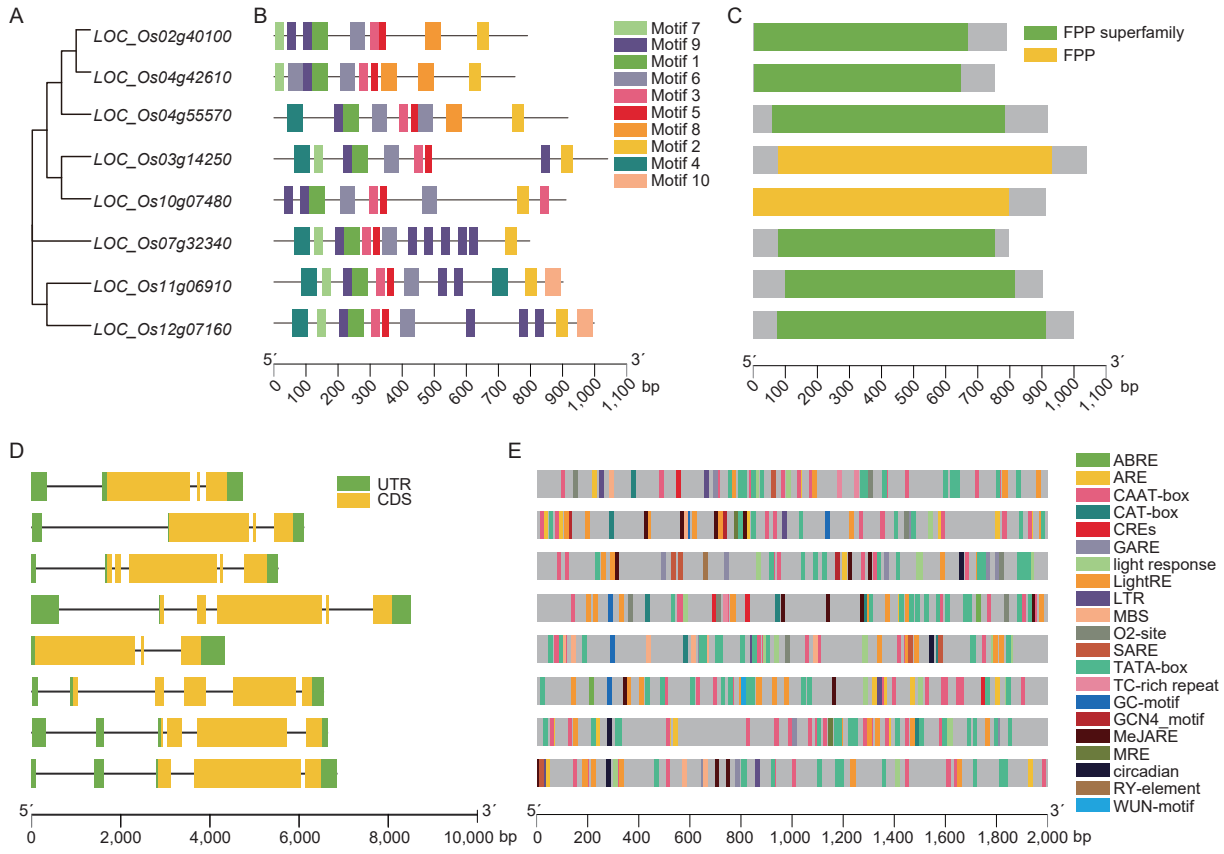


Fig. 2 Phylogenetic relationships, *cis*-acting elements, the architecture of conserved motifs, conserved domains, and gene structures of the filament-like plant proteins (FPPs) from rice. A, OsFPP phylogenetic tree. B, distribution of multiple EM for motif elicitation (MEME)-constructed conserved motifs. Different colored boxes represent various conserved motifs (motifs 1–10). C, conserved domains of OsFPPs. D, OsFPP exon/intron structures. Black lines represent introns, yellow boxes signify exons, and green boxes indicate 5′-untranslated region (UTRs). E, distribution of *cis*-acting elements in the 2 kb upstream sequence of OsFPPs, with element types color-coded.

(Fig. 2-D). This finding likely reflects the possibility of alternative splicing in *OsFPPs*.

Moreover, a 2,000 bp promoter sequence was examined for *cis*-acting elements (Fig. 2-E; Appendix F). The majority of these elements consisted of light-responsive *cis*-regulatory elements (such as MRE, LightRE, and light response elements), transcriptional regulatory elements (such as CREs, CAAT-box, and TATA-box), and hormone-related elements (like ABRE (ABA-responsive element), salicylic acid-responsive element (SARE), gibberellin-responsive element (GARE), and methyl jasmonate response element (MeJA)). A significant number were also represented by other categories, which included developmental elements, stress-related elements, meristem expression elements, and others (such as ARE (anaerobic induction element), TC-rich repeats, CAT-box, GC-motif, GCN4 motif, WUN motif, MYB-binding site (MBS), and low-temperature-responsive element (LTR)). Therefore, the *OsFPPs* can react to a range of hormones and stresses based on the presence of *cis*-acting factors. These response factors may directly influence the ability of OsFPPs to respond to stress.

3.3. The *OsFPPs* reactions to abiotic stress and hormones

To shed light on the possible roles of *OsFPPs*, their expression patterns were initially examined under treatment with abiotic stressors and hormones (exogenous ABA, MeJA, drought, flood, and cold stress). The findings indicated changes in the expression levels of the majority of *OsFPPs*. Under all abiotic stress conditions and hormone treatments, the majority of *OsFPP* members exhibited pronounced declines. Thus, the expression levels of *OsFPPs* are stimulated by multiple abiotic stresses and hormones (Appendix G).

In addition, the predicted interaction networks of AtFPPs and OsFPPs were constructed separately (Appendix G). Seven AtFPPs were predicted to form a complex network, and four OsFPPs were connected. AtFPP2 and AtFPP3 exhibited a strong interaction with the COG family genes. AtFPP7 showed a strong and indirect correlation with the branched-chain-amino-acid aminotransferase (BCAT) family and a direct correlation with members of the isopropyl malate synthase (IPMS) family. LOC_*Os02g40100*, LOC_*Os04g42610*, and LOC_*Os04g55570* showed strong correlations with enzymes involved in the synthesis pathways of mitochondrial NAD-dependent isocitrate dehydrogenase (*IDHc;1*, *OsIDHc;2*, and *OsIDHa*) or pyridoxal-phosphate-dependent aminotransferase. Meanwhile, LOC_*Os07g32340* clustered together with enzymes involved in the glutamyl amidotransferase and aminoacyl synthetase family.

3.4. OsFPP7 shows multiple organelle localization and C-terminus-mediated transcriptional repression

Abiotic stress-related motifs such as TC-rich, ABRE, LTR, and MBS are simultaneously present in the promoter of LOC_*Os02g40100*. Its expression is significantly suppressed by treatments such as drought, flooding, low temperature, and exogenous ABA. Therefore, based on the expression pattern and number of abiotic stress response components, LOC_*Os02g40100* was selected as a gene for further research. We named LOC_*Os02g40100* as *OsFPP7* based on the description of "filament-like plant protein 7" from NCBI (GeneBank: XP_015623448.1). A systematic evolutionary analysis showed that *OsFPP7* is highly homologous to sequences in multiple monocotyledons (Appendix H). Consistent with the collinearity analysis results (Fig. 1-B; Appendices C and H), sequence alignment revealed that OsFPP7 is highly conserved with all other FPP7 proteins in monocotyledons but not with those in *Arabidopsis*. Furthermore, *OsFPP7* has an nuclear localization signal (NLS) sequence in its C-terminal area and two PF05911 domains in its N-terminal area (Appendix H).

OsFPP7 was found to be highly expressed in the sheath during the vegetative stage and in stems and roots during the reproductive stage, as indicated by a spatiotemporal distribution analysis (Fig. 3-B). Subcellular localization shows that in addition to the nucleus, as anticipated, the cytosol and plasmalemma also contained the fluorescent signal (Fig. 3-D). As shown in Fig. 3-C, strains transformed with full-length OsFPP7 are unable to grow on the selective media. Notably, we also observed that the N- and C-termini of OsFPP7 exhibit opposing transcriptional activities: the N-terminus (the first FPP Pfam) confers transcriptional activity to *OsFPP7*, while the C-terminus confers inhibitory activity.

3.5. *OsFPP7* negatively regulates salt tolerance and enhances ABA sensitivity in rice

The phytohormone ABA is essential for many physiological functions that occur in plants during growth and in response to abiotic stresses (Guilfoyle *et al.* 2015). To explore whether *OsFPP7* affects ABA signaling in rice, we generated independent CRISPR/Cas9 lines in the WT (ZH11) background. A frameshift variation resulting in an early stop codon was observed in the *ko1* mutant. This mutation was caused by a 32 bp deletion located 28 bp downstream of the start codon ATG. A 1 bp deletion located 30 bp downstream of ATG in the *ko2* mutant also resulted in a frameshift variation and an early stop codon (Appendix I). *OsFPP7* exhibited overexpression (OE) in the same background (Fig. 4-K). Two homozygous OE lines (OE3 and OE10) and KO lines (*ko1* and *ko2*) were used to assess the phenotypic impact. No phenotypic differences were observed among all genotypes under the control conditions, but the fresh weight of OE3 was lower than the others. When exposed to exogenous ABA, compared to WT, the shoot length, root length, and fresh weight of the *ko* lines were significantly increased, while they were suppressed in the OE lines (Fig. 4-A). These results suggest that during the germination stage, ABA sensitivity is greater in the *OsFPP7* OE lines.

Plant resistance to salinity stress is also influenced by ABA signaling regulators (Li *et al.* 2022). The relative transcript levels of *OsFPP7* under NaCl treatment were measured using qRT-PCR, which demonstrated substantial repression of *OsFPP7* expression (Fig. 3-A). How *OsFPP7* functions biologically under salt stress was also determined (Fig. 4-B–D). The fresh weight, shoot length, and root length (Fig. 4-B–D) were enhanced in the *ko* lines compared to WT, while they declined in the OE lines. These findings imply that *OsFPP7* has a detrimental effect on salt stress resistance at the rice budding stage. Meanwhile, the root length, fresh weight, and shoot length were further suppressed by treatments with NaCl and ABA, and the *ko* lines were only slightly inhibited compared to the others, which may have contributed to the enhanced salt-tolerance ability. We also assessed the salt tolerance of rice by examining all genotypes of *OsFPP7* at the seedling stage. Most of the leaves of the OE lines were markedly wilted, and seedlings of the *ko* lines were less affected compared with the WT (Fig. 4-E). Statistics showed that the *ko* lines had significantly longer roots and a higher survival rate than the OE lines, which exhibited noticeable declines in fresh weight and shoot length (Fig. 4-F–J). These results suggest that *OsFPP7* negatively regulates salt stress. Furthermore, the OsFPP7 OE lines appeared to be shorter in stature than the WT lines (Appendix J). However, the effective panicle number, yield per plant, spike length, and setting percentage of the OsFPP7 OE lines showed no significant differences compared to those of the WT lines. Moreover, the knockout of OsFPP7 showed no differences in major agronomic traits (Appendix J).

3.6. *OsFPP7* affects the ion and ROS homeostasis of rice seedlings under salt stress

One crucial adaptation characteristic of salt-tolerant plants is their ability to maintain cellular ion homeostasis in response to excess ions (Yang and Guo 2017). The Na^+ and K^+ concentrations of seedlings cultivated hydroponically were measured. The Na^+ levels were low in the shoots of all genotypes under normal conditions; but, following exposure to salt stress, they significantly rose. There was little variation in the K^+ content (Appendix I). Compared to WT, the OE lines had higher Na^+ concentrations during salt stress (Fig. 5-A). As for the massive Na^+ accumulation in the shoots, the Na^+/K^+ ratios were significantly enhanced in the OE lines, but significantly lower in the *ko* lines (Fig. 5-B). These findings suggest that under salt stress, *OsFPP7* may have an impact on ion homeostasis.

Plants experience oxidative damage when exposed to salt stress. One of the key strategies for reducing oxidative stress caused by salinity is the ability to scavenge ROS (Bose *et al.* 2013). NBT and DAB staining were performed on the rice seedling leaves of different genotypes to investigate the production of ROS hydrogen peroxide (H_2O_2) and superoxide ($O_2^{-}\cdot$). Under normal conditions, there was no discernible difference in the accumulation of ROS as indicated by the nitro blue tetrazolium dichloride (NBT) and diaminobenzidine (DAB) staining tests. Under salt stress, the OE plants developed more ROS ($O_2^{-}\cdot$ and H_2O_2) than the WT (Fig. 5-C

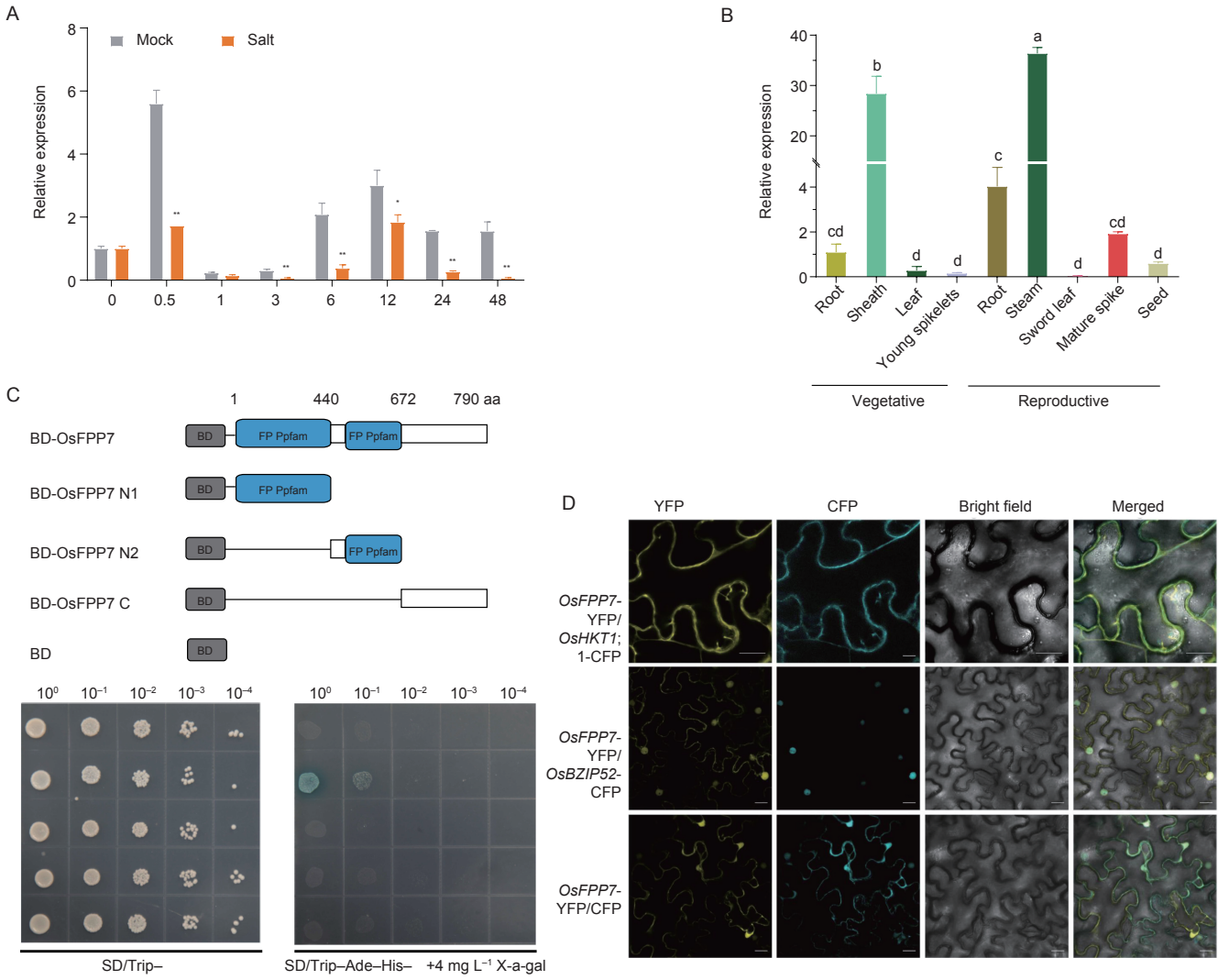


Fig. 3 Expression profiles, transactivation analysis, and subcellular localization of *OsFPP7*. A, qRT-PCR was used to determine the expression levels of *OsFPP7* in shoots of 2-wk-old seedlings that had been exposed to 200 mmol L^{-1} NaCl for the specified durations. Data are presented as mean±SD (n=3). B, *OsFPP7* expression levels were measured using qRT-PCR in various vegetative and reproductive organs during the different growth stages. Bars mean SD (n=3). Different letters (one-way ANOVA Duncan's test, P<0.05) and asterisks indicate significant differences (two-tailed Student's t-test, *, P<0.05 and **, P<0.01). C, analysis of transactivation activity in yeast using various segments and the full-length OsFPP7. pGBKT7 served as the negative control. BD, pGBKT7. D, subcellular localization of *OsFPP7*. *OsBZIP52*-CFP is a marker of nucleus localization (Liu *et al.* 2011), while *OsHKT1;1*-CFP is a membrane marker (Wang *et al.* 2015). The PHB-OsFPP7-YFP and PHB-OsBZIP52-CFP, or PHB-OsHKT1;1-CFP constructs, were co-transformed into tobacco leaves using the *Agrobacterium* infiltration method. PHB-OsFPP7-YFP and PHB-x-CFP were co-transformed into tobacco leaves as a negative control. Signals were detected 3 d after infiltration using a laser confocal 880 microscope. Scale bar in D=10 μm/20 μm.

and D). Malondialdehyde (MDA) levels in the OE plants increased significantly based on the measurements of ROS content (Fig. 5-H), while they were significantly lower in the *ko* lines. Altogether, these data indicate that *OsFPP7* increases the oxidative damage induced by salinity in rice.

The activities of ROS-scavenging enzymes CAT, POD, and SOD, as well as soluble sugar levels, were examined in seedlings with different genotypes under both normal and saline conditions. Under control conditions, the POD and SOD activities of *ko* lines were lower than the WT but surprisingly surpassed them after salt stress. However, compared to WT, the OE plants exhibited lower POD activities and similar SOD activities (Fig. 5-F and G). These findings suggest that by reducing Na^{+} accumulation and increasing ROS-scavenging enzyme activities, the knockout of *OsFPP7* (*osfpp7*) improved salt tolerance.

4. Discussion

The cytoskeleton is essential for stress reactions and signal transduction (Soda *et al.* 2016). The LCC proteins are engaged in cytokinesis, photosynthesis, or defensive mechanisms in plants. The earliest group of plant-specific LCC proteins discovered in the *Arabidopsis* genome, the FPP family, offers a fascinating area of research for understanding the purpose and evolutionary conservation of these functional analogs of animal lamins (Gindullis *et al.* 2002). In this study, we report that *OsFPP7*, a member of the FPP family, is related to rice salt tolerance, which

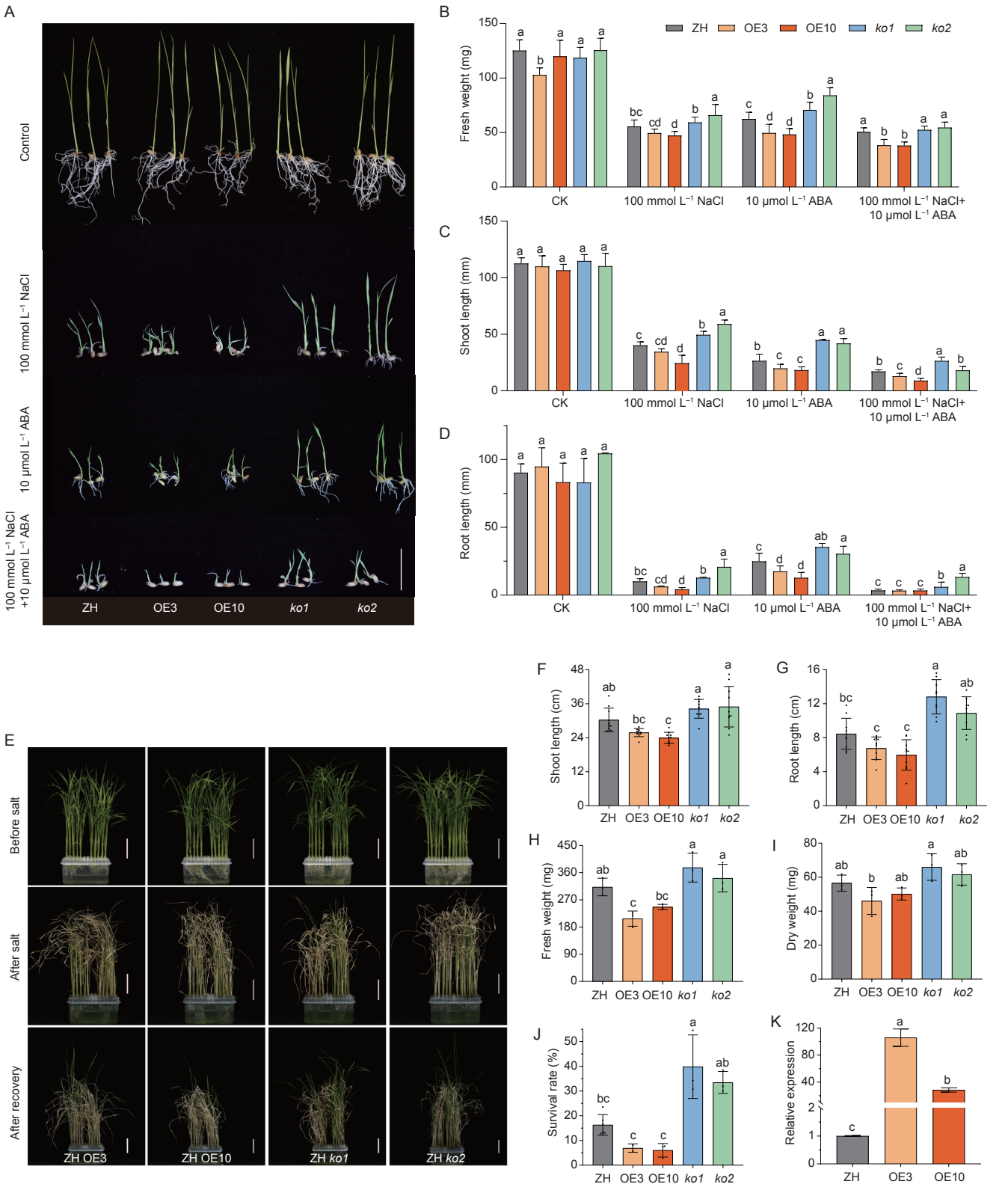


Fig. 4 OsFPP7 negatively regulates rice salt tolerance. A, phenotypes of wild type (WT), *OsFPP7* overexpression (OE) lines (OE3 and OE 10), and *OsFPP7 ko* lines (*ko1* and *ko2*) under various treatment conditions during the germination period. Scale bar=5 cm. B–D, fresh weights, shoot lengths, and root lengths of WT, *OsFPP7* OE lines, and *OsFPP7 ko* lines under various treatment conditions during the germination period. E, phenotypes of WT, *OsFPP7* OE lines and *ko* lines under salt stress during the seedling period. Two-wk-old hydroponically grown seedlings were subjected to a 20-d treatment with 150 mmol L^{-1} NaCl before being allowed to recuperate for an additional 7 d. Three independent biological determinations were conducted, and similar results were obtained. Scale bar=7 cm. F, shoot length. G, root length. H, fresh weight. I, dry weight. J, survival rate. K, qRT-PCR detection of *OsFPP7* transcripts in two independent OE transgenic lines of rice. Bars mean SD (n=10 in B–D, F, and G; n=3 in H–K). Different letters indicate significant differences (one-way ANOVA Duncan's test, P<0.05).

will help us to understand how FPPs function in plant salt tolerance.

4.1. OsFPP7 enhances rice salt stress sensitivity by participating in the ABA signaling pathway

Plant physiology and biochemistry are affected by salt stress throughout the entire developmental period from germination to senescence (Chen *et al.* 2022; Du *et al.* 2023). LCC proteins are known to be involved in abiotic stresses (Bassham *et al.* 2013; Yang *et al.* 2020). The IF protein vimentin is critical for stress tolerance in differentiating stem cells (Pattabiraman *et al.* 2020). Overexpression of the *OsIF* gene improves the growth of transgenic rice plants under salt stress by stabilizing photosynthesis, ultimately increasing plant survival and yield (Soda *et al.* 2018). Overexpression of a lamin-like protein, OsNMCP1, enhances rice drought tolerance (Yang *et al.* 2020). This study showed that the overexpression of OsFPP7 impaired rice salt stress tolerance, and in contrast, the knockout of OsFPP7 enhanced rice salt stress tolerance (Fig. 4), revealing the negative role of OsFPP7 in rice salt stress tolerance.

Given that plant stress responses must be coordinated with growth and development, understanding the crosstalk between the signaling pathways of stress, hormones, and growth is essential. ABA regulates numerous growth and developmental processes in plants from germination to seed dormancy. High concentrations of exogenous ABA inhibit root growth, while low concentrations stimulate primary root growth (Zhang *et al.* 2010). T-DNA insertion mutants and double mutants of the LCC proteins PICC and PICL have shown enhanced sensitivity to the abiotic plant stress hormone ABA in the post-germination growth response (Bassham *et al.* 2013).

Many genes play a role in regulating salt tolerance by controlling ABA signaling pathway genes (Meng *et al.* 2020; Zhang *et al.* 2021). However, little is known about the function of FPP members in the ABA response under salt

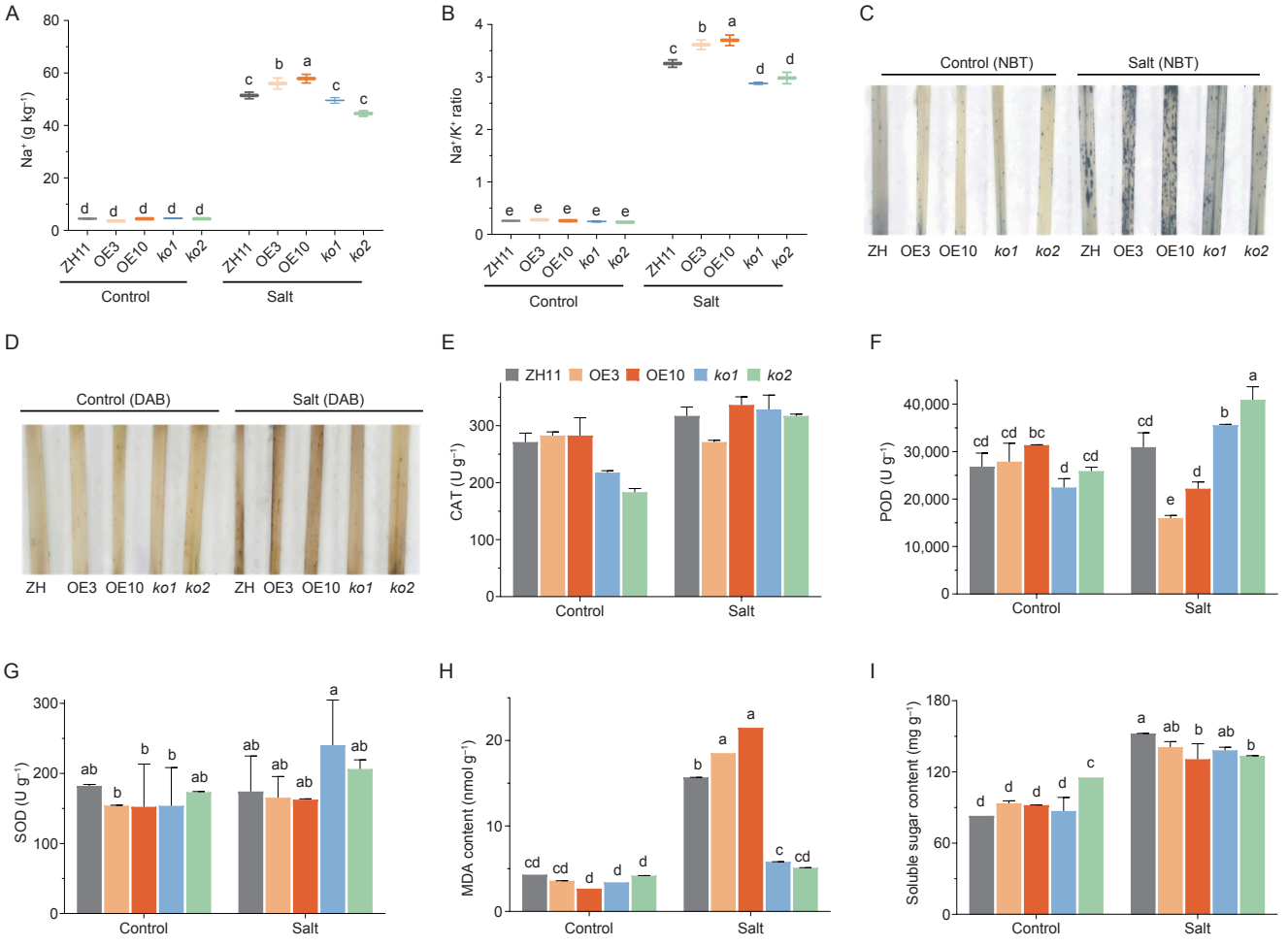


Fig. 5 Physiological and biochemical parameters of 2-wk-old seedlings of the *OsFPP7* overexpression (OE) lines, *ko* lines, and wild type (WT). A and B, total Na^+ contents (A) and Na^+/K^+ ratios (B) of shoots from the designated genotypes were measured after a 13-d salt stress treatment or under normal conditions. For each treatment, three biological replicates involving about 20 plants were assessed. C and D, the seedlings, with or without 150 mmol L^{-1} NaCl treatment for 2 d, were stained with nitro blue tetrazolium dichloride (NBT) (C) and diaminobenzidine (DAB) (D). With 20 plants per treatment, three biological replicates were conducted for each treatment. E–G, contents of catalase (CAT) (E), peroxidase (POD) (F), and superoxide dismutase (SOD) (G) after treatment with 150 mmol L^{-1} NaCl for 1 d. Malondialdehyde (MDA) (H) and soluble sugar (I) contents measured 5 d after treatment with or without 150 mmol L^{-1} NaCl. Bars mean SD (n=3). Different letters indicate significant differences (one-way ANOVA Duncan's test, P<0.05).

stress. This study found a predicted ABRE-responsive and TC-rich repeats element in the OsFPP7 promoter (Figs. 2-E and 3-C). Exogenous ABA treatment suppressed the expression of *OsFPP7* while promoting sheath elongation (Fig. 4; Appendix G). Reduced ABA sensitivity was observed in *osfpp7* plants at the budding stage. Seedlings were significantly inhibited by the combined stresses of salt and ABA, but the same pattern was observed. These results demonstrate that OsFPP7 negatively regulates the salinity stress response by participating in the ABA-dependent signal. Further studies are needed to determine how ABA signaling is perceived and transmitted under salt stress.

4.2. *OsFPP7* plays a negative role in rice salinity stress tolerance by interfering with ionic homeostasis

The accumulation of excess Na^+ and Cl^- in the cells disrupts the original Na^+/K^+ ratio, leading to direct ionic toxicity in the cell membranes and cytoplasm (Munns and Tester 2008). A high concentration of salt ions reduces the water potential of the root surface, hindering water uptake by the plant, which results in osmotic stress and disruption of the intracellular environment. Maintaining cellular Na^+/K^+ homeostasis is crucial for plant survival under salt stress (Yang and Guo 2018). Plants typically employ ion detoxification strategies, such as removing Na^+ from the cytoplasm, transporting Na^+ from root cells to the xylem, and storing ions in vesicles (van Zelm *et al.* 2020). Shoot Na^+ exclusion is essential for ensuring crop salt tolerance (Wang *et al.* 2020). OsIF improves salt stress tolerance and increases yield by maintaining Na^+/K^+ homeostasis (Soda *et al.* 2018).

In this study, the shoot Na^+ content was low and not significantly different in all the genotypes under normal conditions, but it increased sharply under salt stress. Meanwhile, the shoot K^+ concentration decreased slightly but not significantly after salt stress. During salt stress, the OE strain exhibited high accumulation of shoot Na^+, leading to a significant increase in the Na^+/K^+ ratio. In contrast, the *ko* strain displayed a significant reduction in the Na^+/K^+ ratio. This may help maintain ionic homeostasis by facilitating Na^+ efflux. Given its high expression in roots and stems, the direct or indirect regulatory relationship between OsFPP7 and ion transport genes needs further verification.

4.3. Knockout of *OsFPP7* improves rice salt resistance by maintaining ROS scavenging and balance

The ionic imbalance under salt stress further interferes with cellular metabolism, resulting in the generation of large amounts of ROS and secondary oxidative stress. Low levels of ROS can activate the salt stress response, but high concentrations of ROS can damage DNA, carbohydrates, lipids, and proteins, thereby causing cell membrane damage, metabolic dysfunction, and cell death (Apel and Hirt 2004; Miller *et al.* 2010). ROS accumulation in cells during stress affects the redox state of many proteins, alters gene expression, and influences the resilience of plants to stress (Mittler *et al.* 2022). Antioxidant regulation can mediate the removal of ROS and the control and repair of damage; for example, SOD and POD are components of antioxidant enzyme systems (Kärkönen and Kuchitsu 2015). Salt tolerance in saline plants is partly due to an enhanced ability to maintain ROS homeostasis (Bose *et al.* 2013).

A series of genes participate in regulating salt tolerance by enhancing the ROS-scavenging ability through increased antioxidant enzyme activities (Liu *et al.* 2019). As a key member of the ABA signaling pathway, *ABI4* directly binds to two key ROS scavenging genes and regulates ROS metabolism during seed germination under salt stress (Luo *et al.* 2020). *OsAPX2* increases APX activity, reduces H_2O_2 and MDA levels, reduces oxidative stress damage, and enhances rice tolerance to salt stress (Zhang *et al.* 2013). When the level of the LCC protein NECC2 was suppressed, the accumulation of ROS in mouse cells was inhibited (Mu *et al.* 2024). This study demonstrated the detrimental impact of OsFPP7 on rice salt stress tolerance. One of the principal byproducts of cellular oxidation is MDA, which indicates the extent of oxidative damage to cells (Li *et al.* 2022; Zhou *et al.* 2022; Du *et al.* 2023). Consistent with the observations from DAB and NBT staining, *osfpp7* plants accumulated a significantly low level of MDA and exhibited higher POD and SOD activities (Fig. 6). Thus, *osfpp7* enhances salt tolerance in rice through the regulation of ROS homeostasis by enhancing POD activity and reduces oxidative stress damage.

IFs are cytoprotective during oxidative stress by preventing the generation of ROS (Toivola *et al.* 2010; Dutour-Provenzano and Etienne-Manneville 2021). Oxidative stress affects the expression, stability, and posttranslational changes of lamins, which have various impacts on the cells and tissues. For example, laminopathies cause alterations in the expression levels of major antioxidant enzymes (Mao *et al.* 2020). The results of our study reveal, for the first time, that FPPs are involved in regulating plant salt tolerance. We suspect that OsFPP7 may regulate the salt stress response by forming a transcriptional inhibitory complex with partners, such as the relevant genes of POD, the ABA pathway, or ion transport. Furthermore, we hypothesize that OsFPP7 is transported between these compartments, allowing OsFPP7 to act as a cytoskeleton involved in communication within the cytoplasm, plasma membrane, and nucleus. Future studies should aim to clarify the regulatory network mechanisms involving OsFPP7, plant hormones, ROS scavenging, and ion transport.

5. Conclusion

In this study, 59 FPP candidates were identified from four monocots and two dicots, which underwent a relatively conserved evolution in monocots and dicots independently. Furthermore, in rice, OsFPPs are also involved in various abiotic and biotic stressors. Additional genetic evidence showed that *OsFPP7* contributes to salt sensitivity during the germination period by enhancing ABA sensitivity and disrupting the antioxidant and sodium ion transport systems at the seedling stage. The role of the FPP family in regulating salt stress is demonstrated by our findings. Further in-depth studies in this field will advance our knowledge of the cytoskeleton and plant stress tolerance processes while also generating novel concepts for practical applications.

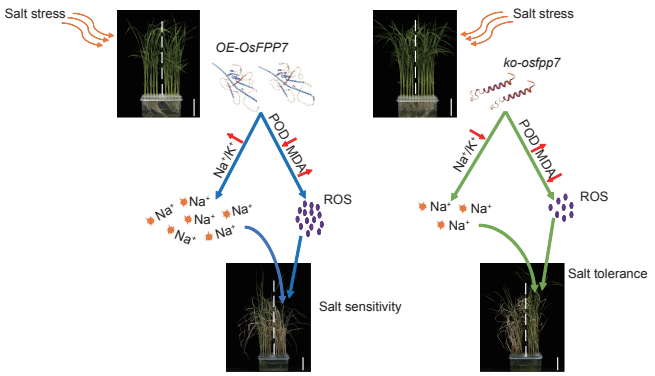


Fig. 6 Proposed working model for the OsFPP7-mediated salt sensitivity of rice seedlings under salt stress. Higher levels of sodium and malondialdehyde (MDA) were present in *OE-OsFPP7* plants, leading to a greater Na^+/K^+ ratio, the accumulation of reactive oxygen species (ROS) and ultimately resulting in a salt-sensitive phenotype. The disrupted protein structure of OsFPP7 hindered the accumulation of sodium and ROS, thereby reducing the oxidative damage caused by salt stress and ultimately improving the salt resistance of seedlings. POD, peroxidase. Scale bars=7 cm.

Acknowledgements

This work was supported by the Science and Technology Innovation Program of Hunan Province, China (2024NK1010 and 2023NK1010), the National Natural Science Foundation of China (U21A20208), the Hunan Seed Industry Innovation Project, China (2021NK1012), the National Key R&D Project of Hunan Province, China (2023NK2002), the Hunan Science and Technology Major Project, China (2023ZJ1080), the Natural Science Foundation of Hunan Province, China (2022JJ40170), and the Major Scientific and Technological Project of Hainan Province, China (ZDKJ2021002).

Declaration of competing interest

The authors declare that they have no conflict of interest.

Declaration of generative AI and AI-assisted technologies in the writing process

The authors declare that they did not use AI in the preparation and writing of this manuscript.

Appendices associated with this paper are available at https://doi.org/10.1016/j.jia.2024.08.029

References

Apel K, Hirt H. 2004. Reactive oxygen species: Metabolism, oxidative stress, and signal transduction. *Annual Review of Plant Biology*, **55**, 373–399.

Bassham D, Venkatakrishnan S, Mackey D, Meier I. 2013. Functional investigation of the plant-specific long coiled-coil proteins PAMP-INDUCED COILED-COIL (PICC) and PICC-LIKE (PICL) in *Arabidopsis thaliana*. *PLoS ONE*, **8**, 57283–57298.

Bose J, Rodrigo-Moreno A, Shabala S. 2013. ROS homeostasis in halophytes in the context of salinity stress tolerance. *Journal of Experimental Botany*, **65**, 1241–1257.

Chen C J, Chen H, Zhang Y, Thomas H R, Frank M H, He Y H, Xia R. 2020. TBtools: An integrative Toolkit developed for interactive analyses of big biological data. *Molecular Plant*, **13**, 1194–1202.

Chen G M, Xuan W, Zhao P Z, Yao X M, Peng C, Tian Y L, Ye J, Wang B X, He J, Chi W C, Yu J, Ge Y W, Li J, Dai Z Y, Xu D Y, Wang C M, Wan J M. 2022. OsTUB1 confers salt insensitivity by interacting with Kinesin13A to stabilize microtubules and ion transporters in rice. *New Phytologist*, **235**, 1836–1852.

Chen L L, Peng Y C, Tian J, Wang X H, Kong Z S, Mao T L, Yuan M, Li Y H. 2016. TCS1, a microtubule-binding protein, interacts with KCBP/ZWICHEL to regulate trichome cell shape in *Arabidopsis thaliana*. *PLoS Genetics*, **12**, 1006266–1006286.

Clark G B, Roux S J, Blumenthal S S D. 2004. Biochemical and immunological characterization of pea nuclear intermediate filament proteins. *Planta*, **218**, 965–975.

Du F, Wang Y, Wang J, Li Y, Zhang Y, Zhao X, Xu J, Li Z, Zhao T, Wang W, Fu B. 2023. The basic helix-loop-helix transcription factor gene, *OsbHLH38*, plays a key role in controlling rice salt tolerance. *Journal of Integrative Plant Biology*, **65**, 1859–1873.

Dutour-Provenzano G, Etienne-Manneville S. 2021. Intermediate filaments. *Current Biology*, **31**, R522–R529.

Flowers T J, Yeo A R. 1995. Breeding for salinity resistance in crop plants: Where next? *Australian Journal of Plant Physiology*, **22**, 875–884.

Gindullis F, Rose A, Patel S, Meier I. 2002. Four signature motifs define the first class of structurally related large coiled-coil proteins in plants. *BMC Genomics*, **3**, 9–19.

Guilfoyle T, Hagen G, Dong T, Park Y, Hwang I. 2015. Abscisic acid: Biosynthesis, inactivation, homoeostasis and signalling. *Essays in Biochemistry*, **58**, 29–48.

Hussain M, Ahmad S, Hussain S, Lal R, Ul-Allah S, Nawaz A. 2018. Rice in saline soils: Physiology, biochemistry, genetics, and management. *Advances in Agronomy*, **148**, 231–287.

Johnson D L, Stiles B L. 2016. Maf1, a new PTEN target linking RNA and lipid metabolism. *Trends in Endocrinology & Metabolism*, **27**, 742–750.

Kärkönen A, Kuchitsu K. 2015. Reactive oxygen species in cell wall metabolism and development in plants. *Phytochemistry*, **112**, 22–32.

Li Y X, Zhou J H, Li Z, Qiao J Z, Quan R D, Wang J, Huang R F, Qin H. 2022. SALT AND ABA RESPONSE ERF1 improves seed germination and salt tolerance by repressing ABA signaling in rice. *Plant Physiology*, **189**, 1110–1127.

Liu C, Wu Y, Wang X. 2011. bZIP transcription factor *OsbZIP52/RISBZ5*: A potential negative regulator of cold and drought stress response in rice. *Planta*, **235**, 1157–1169.

Liu J, Cui L, Xie Z, Zhang Z, Liu E, Peng X. 2019. Two NCA1 isoforms interact with catalase in a mutually exclusive manner to redundantly regulate its activity in rice. *BMC Plant Biology*, **19**, 105–114.

Lu Y M, Tian Y F, Shen R D, Yao Q, Wang M G, Chen M, Dong J S, Zhang T E, Li F, Lei M G, Zhu J K. 2020. Targeted, efficient sequence insertion and replacement in rice. *Nature Biotechnology*, **38**, 1402–1407.

Luo X, Dai Y, Zheng C, Yang Y, Chen W, Wang Q, Chandrasekaran U, Du J, Liu W, Shu K. 2020. The ABI4-RbohD/VTC2 regulatory module promotes reactive oxygen species (ROS) accumulation to decrease seed germination under salinity stress. *New Phytologist*, **229**, 950–962.

Mao X J, Bharti P, Thaivalappil A, Cao K. 2020. Peroxisomal abnormalities and catalase deficiency in Hutchinson-Gilford Progeria Syndrome. *Aging-US*, **12**, 5195–5208.

Meng X, Cai J, Deng L, Li G, Sun J, Han Y, Dong T, Liu Y, Xu T, Liu S, Li Z, Zhu M. 2020. SISTE1 promotes abscisic acid-dependent salt stress-responsive pathways *via* improving ion homeostasis and reactive oxygen species scavenging in tomato. *Journal of Integrative Plant Biology*, **62**, 1942–1966.

Miller G, Suzuki N, Ciftci-Yilmaz S, Mittler R. 2010. Reactive oxygen species homeostasis and signalling during drought and salinity stresses. *Plant, Cell & Environment*, **33**, 453–467.

Mittler R, Zandalinas S I, Fichman Y, Van Breusegem F. 2022. Reactive oxygen species signalling in plant stress responses. *Nature Reviews* (Molecular Cell Biology), **23**, 663–679.

Mu X, Liu S J, Zheng L Y, Ouyang C X, Abdalla A M, Wang X X, Chen K, Yang F F, Meng N. 2024. The long coiled-coil protein NECC2 regulates oxLDL-induced endothelial oxidative damage and exacerbates atherosclerosis development in apolipoprotein $E^{-/-}$ mice. *Free Radical Biology and Medicine*, **216**, 106–117.

Munns R, Tester M. 2008. Mechanisms of salinity tolerance. *Annual Review of Plant Biology*, **59**, 651–681.

Negrão S, Courtois B, Ahmadi N, Abreu I, Saibo N, Oliveira M M. 2011. Recent updates on salinity stress in rice: From physiological to molecular responses. *Critical Reviews in Plant Sciences*, **30**, 329–377.

Oda Y, Iida Y, Nagashima Y, Sugiyama Y, Fukuda H. 2015. Novel coiled-coil proteins regulate exocyst association with cortical microtubules in xylem cells *via* the conserved oligomeric golgi-complex 2 protein. *Plant & Cell Physiology*, **56**, 277–286.

Patel S, Brkljacic J, Gindullis F, Rose A, Meier I. 2005. The plant nuclear envelope protein MAF1 has an additional location at the Golgi and binds to a novel Golgi-associated coiled-coil protein. *Planta*, **222**, 1028–1040.

Pattabiraman S, Azad G K, Amen T, Brielle S, Park J E, Sze S K, Meshorer E, Kaganovich D. 2020. Vimentin protects differentiating stem cells from stress. *Scientific Reports*, **10**, 19525–19539.

Pérez-Sala D, Quinlan R A. 2024. The redox-responsive roles of intermediate filaments in cellular stress detection, integration and mitigation. *Current Opinion in Cell Biology*, **86**, 102283–102296.

Rose A, Manikantan S, Schraegle S J, Maloy M A, Stahlberg E A, Meier I. 2004. Genome-wide identification of *Arabidopsis* coiled-coil proteins and establishment of the ARABI-COIL database. *Plant Physiology*, **134**, 927–939.

Rose A, Schraegle S J, Stahlberg E A, Meier I. 2005. Coiled-coil protein composition of 22 proteomes — Differences and common themes in subcellular infrastructure and traffic control. *BMC Evolutionary Biology*, **5**, 66–86.

Samaniego R, de la Torre C, de la Espina S M D 2008. Characterization, expression and subcellular distribution of a novel MFP1 (matrix attachment region-binding filament-like protein 1) in onion. *Protoplasma*, **233**, 31–38.

Sasaki T, Burr B. 2000. International rice genome sequencing project: The effort to completely sequence the rice genome. *Current Opinion in Plant Biology*, **3**, 138–142.

Seung D, Schreier T B, Bürgy L, Eicke S, Zeeman S C. 2018. Two plastidial coiled-coil proteins are essential for normal starch granule initiation in *Arabidopsis*. *The Plant Cell*, **30**, 1523–1542.

Shimi T, Goldman R D. 2014. Nuclear lamins and oxidative stress in cell proliferation and longevity. In: *Cancer Biology and the Nuclear Envelope*. Springer, New York. pp. 415–430.

Soda N, Gupta B K, Anwar K, Sharan A, Govindjee, Singla-Pareek S L, Pareek A. 2018. Rice intermediate filament, OsIF, stabilizes photosynthetic machinery and yield under salinity and heat stress. *Scientific Reports*, **8**, 4072–4084.

Soda N, Singla-Pareek S L, Pareek A. 2016. Abiotic stress response in plants: Role of cytoskeleton. In: *Abiotic Stress Response in Plants*, Wiley, Hoboken. pp. 107–134.

Sonnhammer E L L, Eddy S R, Durbin R. 1997. Pfam: A comprehensive database of protein domain families based on seed alignments. *Proteins*, **28**, 405–420.

Stefano R, Piera M B. 2001. In situ histochemical monitoring of ozone- and TMV-induced reactive oxygen species in tobacco leaves. *Plant Physiology and Biochemistry*, **39**, 433–442.

Toivola D M, Strnad P, Habtezion A, Omary M B. 2010. Intermediate filaments take the heat as stress proteins. *Trends in Cell Biology*, **20**, 79–91.

De Vos W H, Houben F, Kamps M, Malhas A, Verheyen F, Cox J, Manders E M M, Verstraeten V L R M, van Steensel M A M, Marcelis C L M, van den Wijngaard A, Vaux D J, Ramaekers F C S, Broers J L V. 2011. Repetitive disruptions of the nuclear envelope invoke temporary loss of cellular compartmentalization in laminopathies. *Human Molecular Genetics*, **20**, 4175–4186.

Wang J, Nan N, Li N, Liu Y, Wang T J, Hwang I, Liu B, Xu Z Y. 2020. A DNA methylation reader-chaperone regulator-transcription factor complex activates *OsHKT1;5* expression during salinity stress. *The Plant Cell*, **32**, 3535–3558.

Wang R, Jing W, Xiao L Y, Jin Y K, Shen L, Zhang W H. 2015. The rice high-affinity potassium transporter1;1 is involved in salt tolerance and regulated by an MYB-type transcription factor. *Plant Physiology*, **168**, 1076–1090.

Xu C C, Ji L, Chen Z D, Fang F P. 2021. Analysis of China's rice industry in 2020 and the outlook for 2021. *China Rice*, **27**, 1–4. (in Chinese)

Yang J, Chang Y, Qin Y, Chen D, Zhu T, Peng K, Wang H, Tang N, Li X, Wang Y, Liu Y, Li X, Xie W, Xiong L. 2020. A lamin-like protein OsNMCP1 regulates drought resistance and root growth through chromatin accessibility modulation by interacting with a chromatin remodeller OsSWI3C in rice. *New Phytologist*, **227**, 65–83.

Yang Y, Guo Y. 2017. Elucidating the molecular mechanisms mediating plant salt-stress responses. *New Phytologist*, **217**, 523–539.

Yang Y, Guo Y. 2018. Unraveling salt stress signaling in plants. *Journal of Integrative Plant Biology*, **60**, 796–804.

Van Zelm E, Zhang Y, Testerink C. 2020. Salt tolerance mechanisms of plants. *Annual Review of Plant Biology*, **71**, 403–433.

Zhang H M, Han W, De Smet I, Talboys P, Loya R, Hassan A, Rong H, Jürgens G, Knox J P, Wang M H. 2010. ABA promotes quiescence of the quiescent centre and suppresses stem cell differentiation in the *Arabidopsis* primary root meristem. *The Plant Journal*, **64**, 764–774.

Zhang S Q, Xie, Cheng T. 2007. Study of soil improvement salinity in the past 50 years. *Scientia Agricultura Sinica*, **40**, 3227–3236. (in Chinese)

Zhang X, Long Y, Chen X X, Zhang B L, Xin Y F, Li L Y, Cao S L, Liu F H, Wang Z G, Huang H, Zhou D G, Xia J X. 2021. A NAC transcription factor OsNAC3 positively regulates ABA response and salt tolerance in rice. *BMC Plant Biology*, **21**, 546–558.

Zhang Z G, Zhang Q A, Wu J X, Zheng X, Zheng S, Sun X H, Qiu Q S, Lu T G. 2013. Gene knockout study reveals that Cytosolic Ascorbate Peroxidase 2(OsAPX2) plays a critical role in growth and reproduction in rice under drought, salt and cold stresses. *PLoS ONE*, **8**, e57472.

Zhou H, Zhang F, Zhai F C, Su Y, Zhou Y, Ge Z L, Tilak P, Eirich J, Finkemeier I, Fu L, Li Z M, Yang J, Shen W B, Yuan X X, Xie Y J. 2022. Rice GLUTATHIONE PEROXIDASE1-mediated oxidation of bZIP68 positively regulates ABA-independent osmotic stress signaling. *Molecular Plant*, **15**, 651–670.

Executive Editor-in-Chief Xueyong Zhang
Managing Editor Ning Wang